



HAL
open science

Novel phosphonate-functionalized composite sorbent for the recovery of lanthanum(III) and terbium(III) from synthetic solutions and ore leachate

Yuezhou Wei, Khalid A.M. Salih, Mohammed Hamza, Enrique Rodríguez Castellón, Guibal Eric

► To cite this version:

Yuezhou Wei, Khalid A.M. Salih, Mohammed Hamza, Enrique Rodríguez Castellón, Guibal Eric. Novel phosphonate-functionalized composite sorbent for the recovery of lanthanum(III) and terbium(III) from synthetic solutions and ore leachate. *Chemical Engineering Journal*, 2021, 424, pp.130500. 10.1016/j.cej.2021.130500 . hal-03255693

HAL Id: hal-03255693

<https://imt-mines-ales.hal.science/hal-03255693>

Submitted on 14 Jun 2021

HAL is a multi-disciplinary open access archive for the deposit and dissemination of scientific research documents, whether they are published or not. The documents may come from teaching and research institutions in France or abroad, or from public or private research centers.

L'archive ouverte pluridisciplinaire **HAL**, est destinée au dépôt et à la diffusion de documents scientifiques de niveau recherche, publiés ou non, émanant des établissements d'enseignement et de recherche français ou étrangers, des laboratoires publics ou privés.

Novel phosphonate-functionalized composite sorbent for the recovery of lanthanum(III) and terbium(III) from synthetic solutions and ore leachate

Yuezhou Wei^a, Khalid A.M. Salih^b, Mohammed F. Hamza^{a,b,c,*}, Enrique Rodríguez Castellón^d, Eric Guibal^{e,*}

^a Institute of Resources Utilization and Rare Earth Development, Guangdong Academy of Sciences, Guangzhou 510651, China

^b Guangxi Key Laboratory of Processing for Non-ferrous Metals and Featured Materials, School of Resources, Environment and Materials, Guangxi University, Nanning 530004, PR China

^c Nuclear Materials Authority, POB 530, El-Maadi, Cairo, Egypt

^d Universidad de Malaga, Departamento de Química Inorgánica, Facultad de Ciencias, Malaga, Spain

^e IMT – Mines Ales, Polymers Composites & Hybrids (PCH), F-30319, Ales Cedex, France

A B S T R A C T

A new process of phosphorylation of algal/polyethyleneimine composite beads allows to dramatically increase the sorption of rare earth elements (La(III) and Tb(III), as light and heavy REE elements, respectively). Sorption proceeds through interactions with several functional groups (phosphonate, but also amine, and carboxylate groups). The sorption capacity at optimum pH (pH_0 : 5, pH_{eq} : 4–4.2) reaches $1.44 \text{ mmol La g}^{-1}$ and $1.02 \text{ mmol Tb g}^{-1}$ (increased by 4.5 to 6.7 compared with raw beads). Sorption isotherms are fitted by the Langmuir equation, while fast uptake kinetics (equilibrium within 20–30 min) is described by the pseudo-first order rate equation. Bound metal ions are quantitatively desorbed using a 0.2 M HCl/0.5 M CaCl₂ solution; the recycling of the sorbent for five cycles of sorption and desorption shows high stability of sorption (loss of sorption capacity < 9%) and desorption (efficiency > 99%). The sorbent exhibits a remarkable preference for REEs against Si(IV), Ca (II), and Mg(II). The sorbent is used efficiently for the recovery of REEs from acidic leachates of a sedimentary ore. A global process is designed including acidic leaching, pre-treatment of leachates by U(VI) sorption on quaternary ammonium (QA) resin (about 94% of U content). The outlet solution of QA resin is treated at different pH values: the best results are obtained at pH_0 5 (pH_{eq} : ~4.5). The REEs are selectively recovered from the eluates by precipitation with oxalic acid: the REE-oxalate precipitate retains 70–76% of its content in the acidic leachates. After precipitation of Al(III) and Fe(III) at pH 5, residual uranium is recovered by precipitation at pH 9 (4.3% of metal leached from the ore).

Keywords:

Phosphonate-bearing sorbent based on algal/polyethyleneimine composite
Sorption of rare earth elements
Sorption isotherms and uptake kinetics
Metal desorption and sorbent recycling
Application to U(VI), La(III) and Tb(III)
recovery from acidic leachate of sedimentary ore

1. Introduction

The valorization of mineral resources is a strategic issue for the development of high-tech industries (platinum group metals, and rare earth elements, REEs) and nuclear power industry (uranium and thorium). This is especially important when resources are not rich enough to justify conventional processes [1]. Therefore, many research projects have recently been designed for developing new processes and novel sorbents for the recovery of these strategic metals from low-grade resources [2], wastes [3] or effluents [4]. In addition, the potential toxicity of these metallic contaminants to water bodies constitutes a strong incentive for developing alternative materials for the

decontamination of industrial effluents [5–9].

Inspired from conventional industrial resins bearing a wide range of functional groups [10], research has been recently drawn on the design of new sorbents functionalized with the same reactive groups based on natural materials (agro-resources, biopolymers) [11–13], algal resources [14–16], or alternative materials such as carbon-based supports [17], and minerals [18–20]. For example, functional groups such as amidoxime [21], sulfonic [22], aminocarboxylic moieties and aminoacids [23,24], amine [25], imidazole [26] and phosphorus-based reactive groups [27,28] have been immobilized on mineral sorbents, metal organic frameworks, biopolymers or renewable materials (of biological origin). More specifically, this strategy was adopted to functionalize an

* Corresponding authors.

E-mail addresses: m_fouda21@hotmail.com (M.F. Hamza), eric.guibal@mines-ales.fr (E. Guibal).

amine-rich composite synthesized by interaction of alginate (and/or brown algal biomass) with polyethyleneimine. A series of new sorbents bearing amidoxime (for Sr(II) removal) [29], sulfonic acid (for Sc(III), Ce(III) and Ho(III) uptake) [30], quaternary ammonium groups (for As (V) [31], U(VI) [32], and Sc(III) recovery [33]) was recently reported.

Recently, a new process was designed for grafting phosphonate groups on the same type of sorbent [34]. The material (herein called A_1PEI) is activated with epichlorohydrin before processing the phosphorylation (with triethyl phosphite), followed by the de-esterification of the intermediary product to produce a phosphonate-bearing sorbent (POH- A_1PEI). The material was fully characterized and the effect of pH on the recovery of two rare earth elements (REEs) belonging to light and heavy REEs: La(III) and Tb(III), respectively, was tested.

Recently, Opere et al. [35] reviewed the techniques of separation of REEs (together with the most important uses of these strategic metals). In the case of lanthanum, they report the intensive use of La for catalyst synthesis ($\approx 75\%$), ceramic, glass and polishing ($\approx 10\%$). For terbium, the principal uses focus on optical systems (laser, optical fibers, medical imaging, cathode ray tubes, liquid crystal displays, about 10% of REEs' uses) and the manufacturing of alloys ($\approx 5\%$ of REEs' uses). On the scale of relative supply risk elaborated by British Geological Survey and reported in the RSC Periodic Table [36]; the two REEs are ranked 9.5 (the highest risk rate being 10). Both of them have recycling rates below 10%; poor substitutability. Most of the reserves (about 50%) are retained in a limited number of countries, while about 97% of the production is operated by 3 top players countries (including China, Russia and Malaysia). These facts readily explain that these REEs are strategic both for high tech development and for geopolitical considerations. Costis et al. [37] recently published a comprehensive review on the occurrence and recovery of REEs from different mining sources (including acid mine drainage, phosphate rocks, etc.) and waste materials (such as red mud, batteries, magnets and waste electric and electronic equipments, WEEEs). WEEEs represent very attractive resources for the production and valorization of REEs [38,39].

These preliminary results [34] confirm that the functionalization of the support significantly improves the sorption properties of the sorbent; this preliminary characterization justifies a more complete investigation of its sorption properties. To more accurately measure the benefit of the functionalization of A_1PEI , the sorption of these two REEs on both A_1PEI and POH- A_1PEI is investigated through the detailed study of pH effect, sorption isotherms and uptake kinetics (both in mono and bi-component solutions), sorption selectivity (from multi-component solutions, in function of pH), metal desorption (desorption kinetics) and sorbent recycling. In the last part of the study, the functionalized sorbent is applied to the treatment of an acidic leachate of Egyptian ore collected in a sedimentary mining basin (representative of a complex medium containing a wide range of different metals). Leachates are pre-treated with a quaternary ammonium ion-exchange resin (for removing uranium) before applying the POH- A_1PEI sorbent (at different pH values). The acid eluates of metal-loaded resins are treated by oxalic acid precipitation for selective recovery of REEs [40]. The residual effluent is treated by precipitation at pH 5 (for iron and aluminum separation) and at pH 9 (for uranium recovery).

The first objective of this study consists in the evaluation of the sorption and desorption properties of the novel sorbent for the La(III) and Tb(III) recovery. The second objective focuses on the design of a complete process for the recovery of REEs from Egyptian ore; including a step of metal sorption on the functionalized A_1PEI beads.

2. Materials and methods

2.1. Materials

Algal biomass (*Laminaria digitata*) was kindly supplied by Setalg (Pleubian, France). After grinding, algal biomass was sieved and particles below 250 μm were used for preparing the raw beads. Branched

polyethylenimine (PEI, $MW_n: \approx 70000 \text{ g mol}^{-1}$, 50%, w/w in water) and glutaraldehyde (GA, 50%, w/w in water) were supplied by Sigma-Aldrich (Taufkirchen, Germany). Polyethylene glycol diglycidyl ether, triethyl phosphite, epichlorohydrin (ECH) and trimethylsilyl bromide were purchased by Shanghai Maklin Biochemical Co., Ltd. (Shanghai, China). Dichloromethane was supplied by Xilong Scientific Co., Ltd., (Guangdong, China). Ethanol (absolute) and sodium hydroxide were purchased from Guangdong Guanghua Sci-Tech (Guangzhou, China). Lanthanum(III) sulfate and terbium(III) sulfate were supplied by National Engineering Research Centre of Rare Earth Metallurgy and Functional Materials Co., Ltd, China. Silicon standard solution (1000 ppm, used as the source for Si) was supplied by Guobiao Inspection and Certification Co. Ltd. (Huairou District, Beijing, China). The other reagents were Prolabo products (VWR, Radnor, PA, USA).

2.2. Synthesis of functionalized sorbent

The method for sorbent synthesis was extensively described in another recent work [34]. Scheme S1 (see [Supplementary Information](#)) reports the synthesis steps for manufacturing POH- A_1PEI . As a brief reminder, the main steps are summarized below.

(a) Synthesis of algal/PEI beads (A_1PEI) – Grinded algal biomass was dispersed under agitation in a sodium carbonate solution at 50 °C for 24 h (to partially extract alginate from algal cell wall). In a second step, 5.35 g of PEI were added to the suspension under agitation for 5 h. The suspension was then dropped wisely into a calcium chloride solution (for ionotropic gelation of carboxylic groups on alginate fraction), completed with glutaraldehyde (for crosslinking of amine groups on PEI chains). After water washing, the beads were freeze-dried. The multiple interactions between amine groups and aldehyde (from GA) and/or carboxylate groups (from alginate), and between carboxylate groups and calcium ions contribute to the stability of the composite beads.

(b) Epichlorohydrin activation of A_1PEI beads (Cl- A_1PEI) – The A_1PEI beads were soaked into ethanol/water solution before adding poly(ethylene glycol) diglycidyl ether (crosslinker, for increasing the strength of the beads) and heating the suspension at 80 °C for 5 h. After this preliminary step, the beads were transferred to another ethanol/water solution completed with epichlorohydrin. Epichlorohydrin may be used (in alkaline solution) for crosslinking supports through the cross-effects of epoxy and chlorine groups; here ECH is used as a spacer arm group that favors the grafting of phosphonate (the same reaction was used for grafting other functional groups) [41]. The reactor was maintained under reflux at 82 ± 3 °C for 3 h. The beads were washed with ethanol and water before being dried in vacuum.

(c) Phosphorylation of Cl- A_1PEI beads (P^*-A_1PEI) – Activated beads were dropped into triethyl phosphite under agitation, maintaining the temperature at 130 °C for 24 h. After being filtrated, the beads were washed with hot water and ethanol and finally dried in vacuum overnight.

(d) De-esterification of P^*-A_1PEI beads (POH- A_1PEI) – Phosphorylated beads were soaked into dichloromethane for 24 h at room temperature, under agitation. The addition of trimethyl silyl bromide allows the de-esterification of phosphoryl groups for producing phosphonate moieties. The reaction took place, under stirring, at 33 ± 2 °C for 24 h. The beads were finally washed with hot water, ethanol, and dried overnight in vacuum.

2.3. Characterization of materials

The morphology observation and the semi-quantitative surface analyses were obtained on a Phenom ProX scanning electron microscope (SEM, Thermo Fisher Scientific, Netherlands) coupled with EDX facilities. The textural properties of the sorbents have been qualified using the BJH method and a Micromeritics TrisStar II (Norcross, GA, USA). Samples were degassed at 100 °C for 12 h, prior to textural characterization.

2.4. Metal sorption from synthetic solutions

Sorption tests were performed with the batch method. A fixed amount of sorbent (m, g) was mixed with a fixed volume (V, L) of solution at a specific concentration (C_0 , mmol L⁻¹) and pH (variable for pH study, or optimized pH value, see below). The precise experimental conditions are systematically reported in the caption of the figures. Agitation was maintained at 170 rpm, while the standard room temperature was $T: 21 \pm 1$ °C. After equilibrium (or fixed sampling times), a sample was collected and filtered through a filter membrane before analyzing the metal content (C_{eq} , mmol L⁻¹) by ICP-AES (inductively coupled plasma atomic emission spectrometer, ICPS-7510 Shimadzu, Tokyo, Japan). The sorption capacity (q_{eq} , mmol g⁻¹) was deduced from concentration variation by the mass balance equation $q_{eq} = (C_0 - C_{eq}) \times V / m$. Similar procedures were used for investigating the sorption of REEs from multi-metal solutions (equimolar concentration: 1 mmol L⁻¹). The tests for metal desorption were also performed in a batch reactor. The samples of sorbents loaded with metal ions were collected from uptake kinetic experiments. The eluent was an acidic calcium chloride solution (i.e., 0.2 M HCl/0.5 M CaCl₂). The sorbent dose (SD, g L⁻¹) was set at 0.8 g L⁻¹. In the investigation of sorbent recycling, a rinsing was systematically performed between each step. Comparison of the amounts of metal sorbed and released was used for calculating the sorption capacity and the desorption efficiency.

The uptake kinetics and sorption isotherms were fitted by conventional equations summarized in Table S1a (pseudo-first order rate equation, PFORE, pseudo-second order rate equation, PSORE, resistance to intraparticle diffusion, RIDE) and Table S1b (Langmuir, Freundlich, and Sips equations) (see [Supplementary Information](#)). The quality of curve fitting was evaluated using the determination coefficient (i.e., R²) and the Akaike Information Criterion (AIC) [42].

Sorption isotherms and uptake kinetics were also performed using POH-A₁PEI at different complementary temperatures (i.e., 32 ± 2 , 42 ± 2 and 52 ± 2 °C) under the same experimental conditions as were for the standard temperature (i.e., 22 ± 2 °C).

The thermodynamic parameters (i.e., ΔH° , enthalpy change, kJ mol⁻¹; ΔS° , entropy change, J K⁻¹ mol⁻¹; and ΔG° , Gibbs free energy change, kJ mol⁻¹) were obtained from the van't Hoff equation:

$$b_L^* = \text{Exp} \left[\frac{-\Delta G^\circ}{RT} \right] \quad (1a)$$

$$\Delta G^\circ = \Delta H^\circ - T\Delta S^\circ \quad (1b)$$

Non-linear form of the van't Hoff equation:

$$b_L^* = \text{Exp} \left[\frac{\Delta S^\circ}{R} - \frac{\Delta H^\circ}{R} \times \frac{1}{T} \right] \quad (1c)$$

Linear form of the van't Hoff equation:

$$\ln b_L^* = \frac{\Delta S^\circ}{R} - \frac{\Delta H^\circ}{R} \times \frac{1}{T} \quad (1d)$$

where b_L is the Langmuir constant converted to its dimensionless expression, and R is the universal gas constant (8.314 J K⁻¹ mol⁻¹). Lima et al. [43] discussed the numerous mistakes appearing in the literature about the calculation of thermodynamic constants. They demonstrated the necessity to use the dimensionless value of the Langmuir parameter (deduced from complete sorption isotherms at a minimum of 4 different temperatures). The dimensionless value of b_L (herein noted b_L^*) should be expressed in L mol⁻¹ and be multiplied by the molality of the solvent (herein water; i.e., 55.51 mol L⁻¹). To be even more accurate, they pointed out the importance of taking into account the activity of the sorbate (γ , dimensionless). In a first approximation, the low concentrations used for the study of sorption isotherms allow considering that $\gamma \approx 1$. The same procedure was used by Kegl et al. [44] for describing thermodynamic behavior for Dy(III) sorption. More

recently, Lima et al. [43] compared the values of thermodynamic parameters when calculated with the linearized and non-linear forms of the van't Hoff equation; they concluded that the differences are relatively limited and that the non-linear method shows slightly higher values for the thermodynamic parameters. For the fitting of experimental profiles, the linear regression was used.

The isosteric heat of sorption ($\Delta H_{isost.}^\circ$, kJ mol⁻¹) is derived from the Clausius-Clapeyron equation [45]:

$$\frac{\partial(\ln C_{eq})}{\partial T} = \frac{-\Delta H_{isost.}^\circ}{RT^2} \quad (2)$$

The isosteric heat of sorption is obtained as the slope ($\Delta H_{isost.}^\circ/R$) of the plots of $\ln C_{eq}$ vs. $1/T$; C_{eq} being calculated from Langmuir equation for different fixed sorption capacities (i.e., q_{eq} : 0.25, 0.5, 0.75 and 1 mmol g⁻¹), at the different temperatures.

For the evaluation of activation energy (E_a , kJ mol⁻¹), the Arrhenius equation was used [46]:

$$\ln k = -\frac{E_a}{R} \times \frac{1}{T} + \ln A \quad (3)$$

where k is the selected rate constant (here in the rate constant obtained from PFORE modeling; the value of apparent rate coefficients was converted in s⁻¹) and A is the frequency factor of the reaction.

2.5. Treatment of Egyptian ore

2.5.1. Egyptian ore characteristics

The Egyptian ore from El-Gor area (Sinai- Egypt) is mainly constituted of gibbsite-bearing shale and claystone (Table S2a). It was characterized by a combination of acid digestion (using concentrated HCl, HNO₃ and HF). A fixed amount (i.e., 0.5 g) of ore mineral (quartered from stock of sieved ore) was digested with HF until maximum dissolving of Si mineral fraction. After evaporation, a mixture of HCl and HNO₃ acids was added under continuous heating for digesting the residual minerals and dissolve the metal ions. Few drops of H₂O₂ were also used for mineralizing the organic materials. These steps were performed in a Teflon beaker at 120–150 °C. The leachate (separated by filtration) was diluted to a volume of 100 mL using deionized water. The metal contents were determined by spectrophotometry using the ammonium metavanadate method for U determination [47], molybdate and molybdovanadate methods for Si and P₂O₅ analyses, respectively, and Arsenazo method for global REE index [48]. A UV-160 spectrophotometer (Shimadzu, Kyoto, Japan) was used for absorbance reading. Other metal ions were determined using an atomic absorption spectrometer (Unicam 969). The chemical composition of the ore is summarized in Table S2b.

2.5.2. Heap leaching

The production of ore leachate was processed using the heap leaching technique. Grinded ore (particle size: 2–8 mm) was treated by percolation of a 50 g L⁻¹ H₂SO₄ solution (~0.5 M): the amount of ore was 5 kg (for an approximate volume of leachate of 4.5 L).

2.5.3. Pre-treatment by sorption on quaternary ammonium resin (QA resin) for U(VI) recovery

The leachate was pre-treated by contact with a commercial ion-exchange resin (QA-Resin, quaternary ammonium/divinylbenzene resin, Rohm & Haas; particle size 0.3–0.9 mm) in batch system for the removal of uranium. Prior to use, the resin (commercially designed under the Cl-form) was conditioned using 1 M sulfuric acid solution (to improve uranyl extraction) [49]. The sorbent dosage was set to 0.2 g L⁻¹.

2.5.4. Sorption and desorption steps on POH-A₁PEI

The sorption was performed by contact (in batch system) of the pre-treated leachate with POH-A₁PEI at different pH₀ values (pH_{eq}: 1.29,

2.41, 3.38, 3.87, and 4.51) for 5 h; the sorbent dosage was set to 0.2 g L^{-1} at $21 \pm 2 \text{ }^\circ\text{C}$ with an agitation speed of $165 \pm 5 \text{ rpm}$. The sorbent was collected for semi-quantitative analysis for metal content. In a second step, the metal-loaded sorbent was mixed with 0.3 M HCl solution using a sorbent dosage of 10 g L^{-1} for 2 h, at room temperature, and under agitation (v : $165(\pm 5) \text{ rpm}$). These experiments were performed on the samples collected at the different pH sorption values.

2.5.5. Selective recovery of REEs from eluates using oxalic acid precipitation

The eluates (processing from the desorption of sorbents loaded in sorption tests at pH_0 : 4 and 5) were treated by the well-known oxalic acid precipitation method [40]. The eluate (20 mL) was mixed with oxalic acid solution (25%, w/w) at pH 1.2 and a temperature of $30 \text{ }^\circ\text{C}$.

2.5.6. Metal separation from the residue – Precipitation of Al/Fe and precipitation of U(VI)

The residue of oxalic acid precipitation contains substantial amounts of U(VI), Ca(II), Fe(III), Al(III) and Si(IV). To selectively recover the residual fraction of uranium, a polishing treatment was applied. The residual solution (after filtration of REE oxalate precipitate) was successively treated with NaOH solutions to adjust the pH to 5 (for precipitation of iron and aluminum), and finally to pH 9 (for uranium precipitation). After filtration, residual concentrations were analyzed, and the precipitate at pH 9 was collected for semi-quantitative EDX analysis.

3. Results and discussion

3.1. Characterization of materials

Previous study has characterized POH- A_1PEI sorbent through different methods such as FTIR and XPS spectroscopies (to characterize the different steps of the functionalization), and thermogravimetric analysis (TGA, for characterization of the differences between raw and functionalized beads). The pH-drift method showed that the functionalization shifted the pH_{PZC} from 6.82 for A_1PEI to 4.29 for POH- A_1PEI beads. The phosphorylation of A_1PEI was also demonstrated by elemental analysis: P content reached 6.8% (w/w; i.e., $2.2 \text{ mmol P g}^{-1}$), while the relative fraction of nitrogen decreased (from 4.9% w/w; i.e., $3.48 \text{ mmol N g}^{-1}$ to 3.9%; i.e., $2.78 \text{ mmol N g}^{-1}$).

In addition, the textural properties have been characterized by nitrogen adsorption and desorption (BET measurements, Figure S1, see Supplementary Information). The functionalization contributes to reduce the specific surface area from 6.1 to $1.1 \text{ m}^2 \text{ g}^{-1}$ consistently with the decrease of the pore volume (from 0.023 to $0.011 \text{ cm}^3 \text{ g}^{-1}$). This may be explained by the blocking of small pores during the functionalization; therefore, the average pore size increases from 166–155 to 496–307 after chemical modification (a-b: corresponding to values deduced from sorption-desorption branches of the isotherms).

FTIR and XPS spectroscopic methods were also used for the characterization of the interactions between the reactive groups of POH- A_1PEI and REEs metal ions (free, or complexed with sulfate anions). Scheme S2 illustrates these mechanisms.

3.2. Treatment of synthetic solutions

3.2.1. Effect of pH on the sorption of La(III) and Tb(III)

Figure 1 compares the sorption properties of La(III) and Tb(III) for raw and functionalized sorbents. The comparison of the profiles clearly demonstrates the strong improvement in sorption properties associated with the phosphorylation of the sorbent. In the case of A_1PEI , the sorption capacity does not exceed $0.104 \text{ mmol La g}^{-1}$ and $0.055 \text{ mmol Tb g}^{-1}$ in the equilibrium pH range 1–5. On the opposite hand, the phosphorylation of the beads allows increasing sorption capacities up to $0.465 \text{ mmol La g}^{-1}$ and $0.373 \text{ mmol Tb g}^{-1}$, under the same

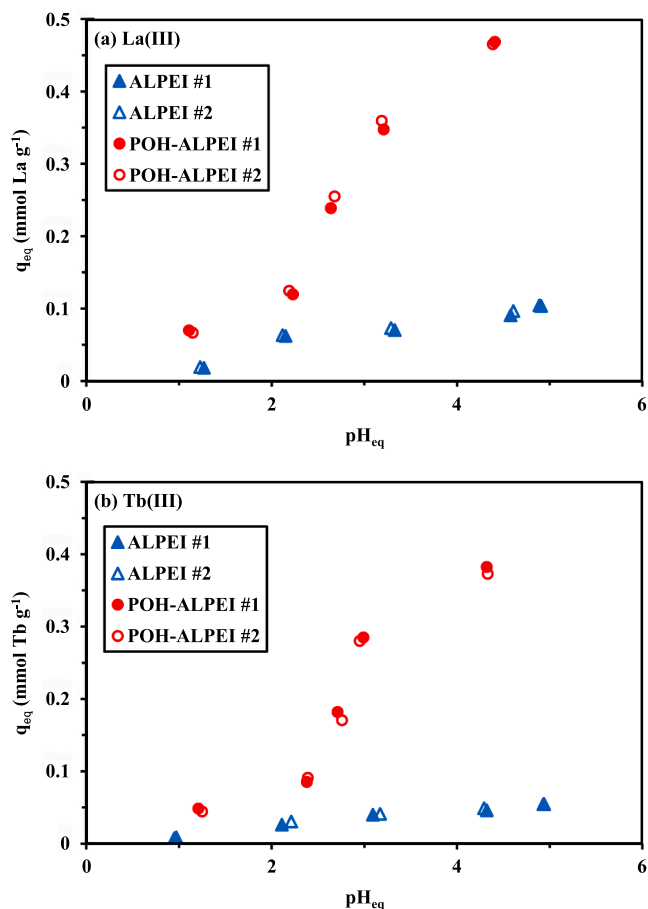


Fig. 1. Effect of equilibrium pH on the sorption of La(III) (a) and Tb(III) (b) using A_1PEI and POH- A_1PEI sorbents (C_0 : $50 \text{ mg L}^{-1} = 0.374 \text{ mmol La L}^{-1}$ or $0.332 \text{ mmol Tb L}^{-1}$; Sorbent dose, SD: 0.66 g L^{-1} ; time: 48 h; T: $21 \pm 1 \text{ }^\circ\text{C}$).

experimental conditions. This significant increase ($\times 4.5$ for La, and $\times 6.8$ for Tb) may be explained by the increase in the density of reactive groups, the higher affinity of phosphonic groups for target metal ions, and the more favorable acid-base characteristics (see pH_{PZC}). As the pH increases, the sorption capacities strongly increase for POH- A_1PEI (especially above pH_{eq} 2.2–2.4); while for A_1PEI , the effect of pH is quickly leveled.

Figure S2 reports the speciation diagrams of lanthanum and terbium under the experimental conditions selected for the study of the pH effect. The predominant species are LaSO_4^+ and TbSO_4^+ below pH 4; between pH 4 and 6, these species co-exist, at comparable levels, with free La^{3+} and Tb^{3+} . The anionic metal disulfate species ($\text{La}(\text{SO}_4)_2^-$ and $\text{Tb}(\text{SO}_4)_2^-$) exist only below pH 3 and never exceed 15–20%. Throughout the pH range investigated in this study, the largely predominant species are cationic. Taking into account that the pH_{PZC} of A_1PEI is close to 4.29, the protonation of the sorbent may explain repulsion effects that limit the sorption efficiency. Charge repulsion decreases with increasing pH and enhances metal sorption. However, even at pH 2, the sorption is not negligible. In addition, despite the negative charge of the sorbent at pH 5, the sorption capacity does not increase dramatically. This probably means that the ion-exchange mechanism is not the main reaction pathway. In the case of POH- A_1PEI , at pH below 2.5, sorption remains very low, below 0.1 – 0.13 mmol g^{-1} (but higher than for A_1PEI). However, at pH above 2.5, a strong increase in sorption is observed, despite the overall positive charge of the sorbent (pH_{PZC} : 6.82). The deprotonation limits the repulsion effect, but this is negligible compared to the strong contribution of new functional groups (phosphonic acid moieties) in the binding of REEs. The binding of metal ions occurs mainly through

chelation on phosphonic groups although carboxylate groups (at pH above pH 4) may also contribute, together with some amine groups (limited number of free groups due to the high yield of grafting). Table S3 shows the semi-quantitative EDX analysis of the sorbent after metal sorption at pH 5. Cl content (atomic fraction) is not affected by metal sorption; the sorption of REEs is confirmed by the appearance of La (2.64% weight concentration, WC) and Tb (WC: 3.09%). Above pH 6, the formation of hydrolyzed species may cause partial precipitation of the metals. Further experiments were performed at pH₀: 5.

Figure S3 shows the log₁₀ plots of the distribution ratio ($D = q_{eq}/C_{eq}$) vs. pH. It is noteworthy that the plots are roughly linear with a slope close to +0.5 for POH-A₁PEI (contrary to A₁PEI, which shows a non-linear variation of log₁₀ D vs. pH). In the case of ion-exchange mechanisms, this slope correlates with the stoichiometric exchange ratio between protons and metal ions (here this would correspond to the exchange of 2 protons per metal ion). Assuming that the REEs are bound through chelation with phosphonic groups; this means that the metal binding proceeds through the release of two protons and the binding of cationic REE species (probably as sulfate species, as confirmed by FTIR and XPS). The coordination numbers of lanthanum and terbium are 9 and 8, respectively [50]. The identification of a supplementary band (assigned to -OH) on HRES for XPS O 1 s signal meant that REE ions are also bonded as solvated species (to complete the coordination sphere) [34].

Figure S4 reports the pH changes during metal sorption. It is noteworthy that the highest changes are observed for POH-A₁PEI, and more specifically in the pH range 3–5 (maximum at pH 4). This is consistent with the titration profiles obtained in the pH-drift method; although the pH variations are less marked in the presence of metal ions. It is also remarkable that, in the pH range 3–4, A₁PEI slightly increases the pH while a reciprocal trend is observed for POH-A₁PEI. This is another evidence of the change in the sorption mechanism for the functionalized sorbent: the release of protons from phosphonic groups during REE sorption decreases the pH (up to 1 unit at pH₀ 4).

3.2.2. Uptake kinetics

Uptake kinetics may be controlled by different mechanisms involving resistances to diffusion (bulk, film and intraparticle diffusion modes), but also thermal exchanges and proper reaction rates. A proper agitation that maintains the homogeneous distribution of the sorbent in the reactor and the homogenous distribution of the solute make it possible to neglect the resistance to bulk diffusion and limit the effect of film diffusion. Reaction rates are frequently associated with pseudo-first and pseudo-second order reaction (PFORE and PSORE, by extension of concepts developed for the modeling of homogeneous kinetics). The experimental profiles (reported in Fig. 2) were fitted by the PFORE, the PSORE (Figure S5), and the RIDE (simplified model of resistance to

intraparticle diffusion, the so-called Crank equation, Figure S6) (Table S1a). Fig. 2 shows that the equilibrium is reached within 20–25 min for POH-A₁PEI, slightly faster than A₁PEI (i.e., 30–35 min). This trend correlates with the greater macro-porosity of the functionalized sorbent that may facilitate the accessibility to the reactive groups (despite the resistance brought by the skin effect of the external layer). The kinetic profiles are roughly similar for La(III) and Tb(III). The higher sorption capacities of the sorbents for La(III) over Tb(III) already observed in the study of pH effect are confirmed by the highest residual concentrations of Tb(III).

The comparison of the models (PFORE, PSORE, and RIDE) (Table 1 and Fig. 2 vs. Figures S5 and S6) shows the marked preference for the PFORE model for fitting experimental profiles compared to PSORE. The PFORE is usually associated with physical sorption (compared with chemical sorption in the case of PSORE). However, a recent work by Hubbe et al. [51] highlighted the importance of appropriate selection of experimental conditions to avoid misinterpretation of these kinetic profiles (and poor understanding of limiting steps). Actually, their review of the literature (screening relevant experimental conditions) demonstrates that the PSORE is frequently misinterpreted as chemical sorption, where actually the limiting mechanism corresponds to resistance to intraparticle diffusion.

The calculated values of the sorption capacities ($q_{eq,1}$) are consistent with the experimental values: the highest dispersion is reported for A₁PEI sorbent (+16% for La(III) and +7% for Tb(III), compared with less than +2% for POH-A₁PEI). As expected, the equilibrium sorption capacities are higher for La(III) than for Tb(III) (~0.465 mmol La g⁻¹ vs. ~0.0376 mmol Tb g⁻¹), and much higher than for A₁PEI (0.121 mmol La g⁻¹ vs. 0.062 mmol Tb g⁻¹). The apparent rate coefficients (k_1) are also higher for POH-A₁PEI compared to A₁PEI (×3.5 for La(III) and ×2.4 for Tb(III)). This is consistent with the decrease in the equilibrium time observed for functionalized sorbent (see above). The apparent rate coefficients are of the same order of magnitude for La(III) (i.e., ~0.168 min⁻¹) and Tb(III) (i.e., ~0.142 min⁻¹).

Despite the lower quality of the curve fit of experimental profiles with the RIDE (especially in the time range corresponding the highest curvature), the model was used to evaluate the order of magnitude of the effective diffusivity coefficient (D_e). Surprisingly, the calculated values of D_e are higher for A₁PEI than for POH-A₁PEI: $2.27\text{--}2.56 \times 10^{-8} \text{ m}^2 \text{ min}^{-1}$ vs. $1.04\text{--}1.40 \times 10^{-8} \text{ m}^2 \text{ min}^{-1}$. The values of D_e are poorly affected by the type of REE. The effective diffusivity is of the same order of magnitude as the free diffusivity of these metal ions in water: $3.71 \times 10^{-8} \text{ m}^2 \text{ min}^{-1}$ for La(III) and $3.42 \times 10^{-8} \text{ m}^2 \text{ min}^{-1}$ for Tb(III) [52]. This confirms that the resistance to intraparticle diffusion does not play the major role in the control of uptake kinetics.

3.2.3. Sorption isotherms

The investigation of sorption isotherms allows evaluating two important parameters: the maximum sorption capacity (obtained at saturation of the sorbent) and the affinity coefficient of the sorbent for the target metal (correlated to the initial slope of the curve representing the sorption capacity as a function of the residual concentration). Fig. 3 shows the sorption isotherms obtained at pH₀ 5 for both La(III) and Tb(III) and both A₁PEI and POH-A₁PEI. The curves are characterized by a saturation plateau starting around 3 mmol L⁻¹ for A₁PEI and around 1.5 mmol L⁻¹ for POH-A₁PEI. The interest of phosphorylation is confirmed by the strong increase in the experimental sorption capacities at sorbent saturation: 0.30 mmol Tb g⁻¹ and 0.43 mmol La g⁻¹ for A₁PEI, increasing up to 1.02 mmol Tb g⁻¹ and 1.44 mmol La g⁻¹ for POH-A₁PEI. The initial slopes are poorly affected by the type of metal, while the slope is significantly increased by the phosphorylation. Sorption isotherms may be fitted by different equations; the most frequently used are the Langmuir equation, the Freundlich equation and the Sips equation. The Freundlich model is associated to an empirical equation that is correlated with multi-layer sorption, possible interactions between sorbed molecules, and heterogeneous distribution of sorption energies. This

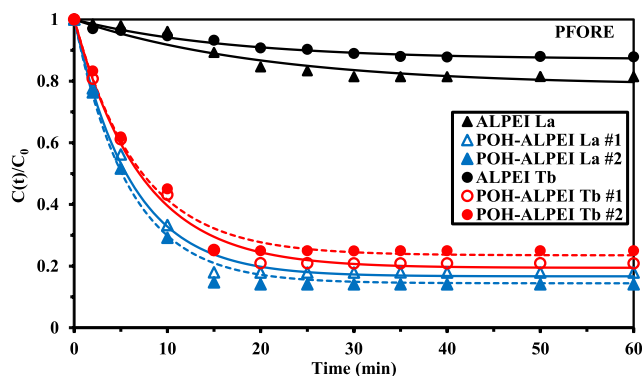


Fig. 2. Uptake kinetics for La(III) and Tb(III) sorption using A₁PEI, and POH-A₁PEI (Lines: modeling with the PFORE; C₀: 0.36 mmol La L⁻¹ or 0.31 mmol Tb L⁻¹; SD: 0.666 g L⁻¹; pH₀: 5; pH_{eq}: 4.8–4.9 for A₁PEI; 4.3–4.5 for POH-A₁PEI; T: 21 ± 1 °C).

Table 1

Uptake kinetics for La(III) and Tb(III) sorption using A_LPEI and POH-A_LPEI sorbents – Modeling parameters.

Model	Parameter	La(III)			Tb(III)		
		A _L PEI	POH-A _L PEI #1	POH-A _L PEI #2	A _L PEI	POH-A _L PEI #1	POH-A _L PEI #2
Exp.	q _{eq,exp}	0.104	0.471	0.459	0.058	0.375	0.377
PFORE	q _{eq,1}	0.121	0.471	0.459	0.062	0.382	0.384
	k ₁ × 10	0.480	1.64	1.71	0.595	1.39	1.45
	R ²	0.943	0.994	0.996	0.979	0.994	0.989
	AIC	-90	-87	-87	-117	-87	-81
PSORE	q _{eq,2}	0.172	0.533	0.518	0.080	0.440	0.441
	k ₂ × 10	2.14	4.05	4.40	7.14	3.96	4.12
	R ²	0.926	0.972	0.974	0.974	0.974	0.965
	AIC	-87	-68	-68	-115	-70	-67
RIDE	D _e × 10 ⁸	2.27	1.22	1.04	2.56	1.17	1.40
	R ²	0.905	0.963	0.965	0.964	0.965	0.958
	AIC	-84	-65	-65	-113	-66	-65

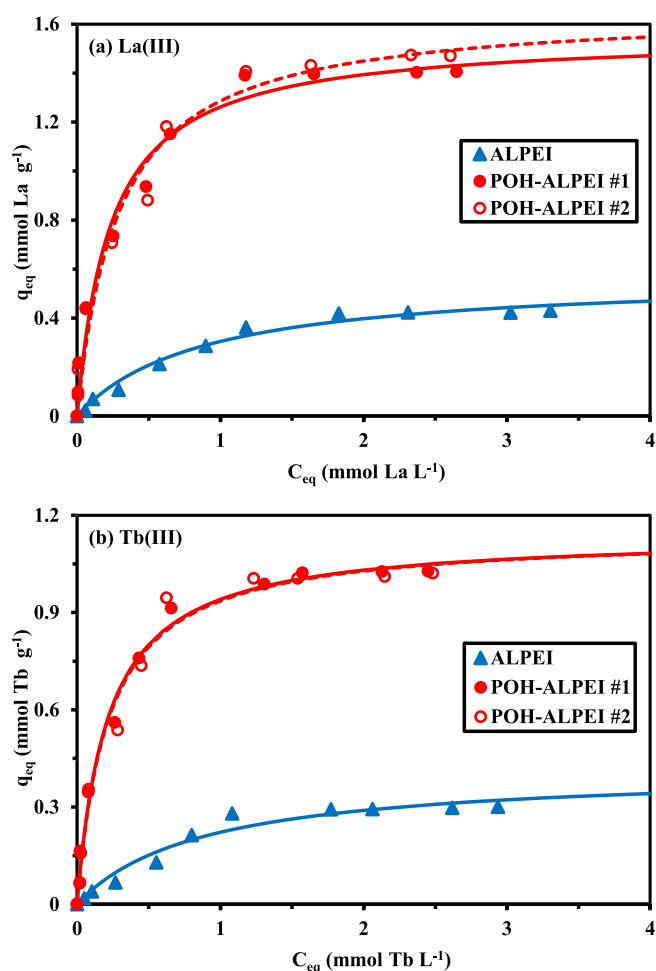


Fig. 3. La(III) (a) and Tb(III) (b) sorption isotherms using A_LPEI, and POH-A_LPEI (Lines: modeling with the Langmuir equation; C₀: 0.07–3.6 mmol La L⁻¹ or 0.06–0.31 mmol Tb L⁻¹; SD: 0.666 g L⁻¹; pH₀: 5; pH_{eq}: 4.89–4.75 for La and 4.96–3.88 for Tb for A_LPEI; 4.51–4.39 for La and 4.37–4.27 for POH-A_LPEI; time: 48 h; T: 21 ± 1 °C).

model is usually represented by non-asymptotic shape of sorption isotherms (associated with the power-type of the equation). Therefore, this model is poorly adapted to current results. The Langmuir equation assumes that sorption occurs as a monolayer without interactions between sorbed molecules and homogeneous sorption energies. The plot of the Langmuir equation is characterized by an asymptotic trend, which is more consistent to the experimental profiles. The Sips equation is actually a combination of Langmuir and Freundlich equations that

allows (with a third-adjustable parameter) to fit better experimental profiles (especially in the concentration range corresponding to a greater curvature). Table 2 shows the parameters of the different models (together with statistical indicators: R² and AIC). In most cases, the Sips equation fits the experimental data better than other models. However, the criterion conventionally used for discriminating two models requires that the |ΔAIC| be >2. Both Langmuir and Sips equations appear to appropriately simulate sorption isotherms. In Fig. 3, the solid lines show the fitted curves. The calculated values of the sorption capacity at saturation of the monolayer (i.e., q_{m,L}) tend to overestimate the experimental maximum sorption capacity; especially for A_LPEI (at + 33–38%, while for POH-A_LPEI the overestimation is limited to + 10–13%). The phosphorylation of the raw material increases (a) the sorption capacity at saturation of the monolayer by a factor 2.8 and (b) the affinity coefficient (b_L) by 3 to 4.1.

The highest sorption capacity and affinity of the two sorbents for La (III) over Tb(III) can be explained by the nature of reactive groups and the softness character of target metals. REEs are part of the so-called hard acids that are supposed to have a greater reactivity with hard bases, according to the Pearson’s rules (Hard and Soft Acid Base theory, HSAB) [53,54]. Phosphonate moieties are considered hard bases [55], these functional groups have a high affinity for REEs. Table S4 reports the main physicochemical characteristics of La(III) and Tb(III): lanthanum as a higher softness parameter, a larger ionic radius (in hydrated form), lower solution electronegativity and lower hydration enthalpy compared with terbium. The increase in sorption properties with phosphorylation can be explained by an increase in the density of the reactive groups (P content in elemental analysis, see above), by the grafting of hard base phosphonic groups onto amine-based moieties, and by the acid-base properties of the two sorbents. Alexandratos and Zhu [56] investigated a series of phosphate-bearing resins for the sorption of different metals in relation with hydrogen bonding effect and reported that an appropriate balance must be found in the yield of hydrogen bonding to optimize the metal sorption.

Table 3 summarizes the sorption properties of alternative sorbents for La(III) and Tb(III) recovery for comparison with A_LPEI and POH-A_LPEI. Literature on terbium sorption is scarce compared with lanthanum. The differences in experimental conditions (especially in terms of pH) make difficult the direct comparison of performances (sorption capacities and equilibrium time); however, these comparisons show some meaningful trends. The two sorbents described in this work are characterized by fast uptake compared to the published literature. Although some sorbents show higher maximum sorption capacities (functionalized MOF [57], magnetic alginate beads [58] or functionalized chitosan [59] for La(III), and functionalized nanofibrous membrane [60] for Tb(III)), POH-A_LPEI demonstrate outstanding combined performances at pH₀ 5 in terms of sorption capacities, affinity coefficients and kinetic characteristics.

Table 2
La(III) and Tb(III) sorption isotherms using A_LPEI and POH-A_LPEI sorbents – Modeling parameters.

Model	Parameter	La(III)			Tb(III)		
		A _L PEI	POH-A _L PEI #1	POH-A _L PEI #2	A _L PEI	POH-A _L PEI #1	POH-A _L PEI #2
Exp.	q _{m,exp}	0.430	1.41	1.47	0.301	1.03	1.02
Langmuir	q _{m,L}	0.573	1.56	1.66	0.416	1.14	1.14
	b _L	1.14	4.27	3.43	1.14	4.72	4.58
	R ²	0.985	0.984	0.981	0.966	0.993	0.981
	AIC	-80	-51	-48	-78	-70	-59
Freundlich	k _F	0.275	1.15	1.17	0.201	0.855	0.853
	n _F	2.16	3.24	3.06	2.05	3.05	3.09
	R ²	0.945	0.964	0.969	0.924	0.944	0.932
	AIC	-65	-44	-45	-69	-46	-44
Sips	q _{m,s}	0.485	1.84	2.10	0.320	1.16	1.17
	b _S	1.89	2.00	1.45	3.06	4.31	3.99
	n _S	0.710	1.46	1.56	0.512	1.04	1.06
	R ²	0.991	0.988	0.984	0.984	0.993	0.981
	AIC	-81	-53	-49	-81	-66	-55

Table 3
La(III) and Tb(III) sorption properties for selected sorbents.

Metal	Sorbent	pH ₀	Time	q _{m,L}	b _L	Ref.
La	<i>Mycobacterium smegmatis</i>	1.5	180	0.024	4.1	[72]
	<i>Pseudomonas aeruginosa</i>	5	180	1.00	n.d.	[73]
	<i>Sargassum polycystum</i>	5	n.d.	0.98	69.4	[74]
	<i>Platanus orientalis</i> leaf	4	60	0.206	18.1	[75]
	<i>Sargassum</i> sp.	n.d.	60	0.66	116	[76]
	Bamboo charcoal	7.2	480	1.38	76.5	[77]
	Iron oxide/alginate beads	5	1680	0.861	0.563	[78]
	<i>Turbinaria conoides</i>	5	120	1.11	5.28	[79]
	<i>Citrus reticulata</i> peel	5	60	1.11	10.6	[80]
	Grapefruit peel	5	60	1.23	5.21	[81]
	Lewatit TP 207	3.6	60	0.867	47.0	[82]
	SnO ₂ /TiO ₂	5	60	0.488	26.4	[83]
	nanocomposites					
	Functionalized calixarene-based membrane	5	1440	1.12	144	[84]
	Magnetic alginate beads	4	300	2.03	0.87	[58]
	Functionalized chitosan	4	240	2.03	0.06	[59]
	Banana peel	5.2	1440	0.279	361	[85]
	SQS-6 strongly cationic resin	4 M H ₃ PO ₄	10	0.086	3.66	[86]
	Purolite S950	0.2 M HNO ₃	180	0.636	12.9	[10]
	Functionalized MOF composite	7	40–60	2.08	44.4	[57]
Graphene magnetic nanoparticles	4	15	0.358	35.4	[87]	
A _L PEI	5	40	0.573	1.14	<i>This work</i>	
POH- A _L PEI	5	40	1.61	3.85	<i>This work</i>	
Tb	Chelating PAPDM hydrogel	7	720	0.466	35.6	[88]
	Functionalized nanofibrous membrane	6	240	1.35	11.0	[60]
	Functionalized hybrid sorbent	8	30	0.124	1.92	[20]
	A _L PEI	5	40	0.416	1.14	<i>This work</i>
	POH- A _L PEI	5	40	1.14	4.65	<i>This work</i>

Time: min; q_{m,L}: mmol g⁻¹; b_L: L mmol⁻¹

3.2.4. Influence of temperature on sorption performance

3.2.4.1. Effect of temperature on sorption isotherms – Thermodynamic parameters. Figure S7 compares the sorption isotherms obtained at

different temperatures to those obtained at T: 22 °C (duplicate experiments); lines correspond to Langmuir modeling of experimental data (using the parameters reported in Table S5). The sorption capacity at saturation (q_{m,L}) increases with temperature (Table S5) for both La(III) and Tb(III). Increasing the temperature favors the sorption of REEs on POH-A_LPEI; the sorption is endothermic. The van't Hoff plots are reported in Figure S8. The dispersion of points (low determination coefficients) means that the thermodynamic parameters deduced from these plots should be considered indicative of the order of magnitude of these parameters. The enthalpy change is slightly higher for Tb(III) than for La(III) (18.56 vs. 16.68 kJ mol⁻¹) (Table S6); the positive value of the enthalpy change confirms the endothermic nature of the sorption process. These values are close to the limit value (around 18 kJ mol⁻¹) commonly used for discriminating between physisorption (<18 kJ mol⁻¹) and chemisorption. The entropy changes are also of the same order of magnitude (158 and 166 J K⁻¹ mol⁻¹ for La(III) and Tb(III), respectively). The positive values of ΔS° are usually associated to an increase in the randomness at the solid/liquid interface after metal sorption. Ceglowski and Schroeder [61] associate this increase in randomness to the possible release of water from hydration layer during metal sorption. The negative values of ΔG° (from -30.0 to -35.4 kJ mol⁻¹) are frequently correlated with the spontaneity of the binding process: this spontaneity increases with the temperature (consistently with the endothermic nature of the mechanism). Similar trends were reported by Botelho et al. [62], Cantu et al. [46] reported that when the Gibbs free energy change ranges between -34 and -40 kJ mol⁻¹, the sorption mechanism is controlled by an ion exchange mechanism. The absolute values of |TΔS°| being superior to |ΔG°|, the sorption is preferentially controlled by entropic effect rather than enthalpic effect.

The isosteric heat of sorption varies between 23.5 and 30.3 kJ mol⁻¹ for La(III) (for sorption capacities: 0.25–1 mmol g⁻¹); much larger differences are observed for Tb(III) (i.e., 21.5–42.6 kJ mol⁻¹) (Figure S9). These values are higher than those reported by Lopčić et al. [45] for copper biosorption (i.e., 12.5–20 kJ mol⁻¹ with sorption capacities in the range 0.05–0.2 mmol Cu g⁻¹).

3.2.4.2. Effect of temperature on uptake kinetics – Energy of activation.

Consistently with the endothermic behavior of REEs sorption onto POH-A_LPEI; the equilibrium concentrations decrease with increasing the temperature and the equilibrium sorption capacities increase. The initial slope of the kinetic curves increases with the temperature. This means that the temperature not only influences the equilibrium but also kinetics. Increasing the temperature favors the mobility of REEs and enhances the mass transfer properties of POH-A_LPEI (Figure S10; lines represent PFORE modeling with parameters summarized in Table 7). Table S7 compares the modeling of experimental profiles with the PFORE, the PSORE, and the RIDE equations. Consistently with the results obtained at T: 22 °C, the PFORE fits better the data than the

alternate models. The rate coefficient k_1 (for the PFORE) clearly increases with the temperature for Tb(III); in the case of La(III), the dispersion of k_1 values makes difficult defining a clear trend. This is confirmed by the Arrhenius plots [46], appearing in Figure S11. The wavy variation of the plot does not allow quantifying the activation energy: the uptake kinetics is poorly affected by temperature. In the case of Tb(III), the variation of the apparent rate coefficient k_1 is also very limited; however, a continuous increase of the apparent rate coefficient can be observed (from 0.139 to 0.96 min^{-1}). The determination coefficient is relatively low (i.e., R^2 : 0.83) but it is possible to roughly evaluate the activation energy close to 7.64 kJ mol^{-1} . Low values ($<40 \text{ kJ mol}^{-1}$) have been associated with fast uptake [63], consistently with the results obtained with POH-A₁PEI. Inglezakis and Zorpas [64] reported the threshold values of activation energy for discriminating between physisorption ($<40 \text{ kJ mol}^{-1}$), ion exchange (24–40 kJ mol^{-1}) and chemisorption ($>40 \text{ kJ mol}^{-1}$). Apparently, the activation energy for Tb(III) sorption onto POH-A₁PEI is low enough to consider the binding as driven by a physisorption mechanism. This appears to be contradictory with the expected chelation mechanism as characterized by FTIR and XPS analyses [34].

3.2.5. Multi-component solutions – Selectivity

Kinetic experiments in binary equimolar La(III)-Tb(III) solutions were carried out with both A₁PEI and POH-A₁PEI beads (Figure S12 and Table S8). The comparison of the profiles shows that for the raw material, the equilibrium is reached slightly faster for Tb(III) than for La(III). This is confirmed by the apparent rate coefficient for PFORE (Table S5): k_1 increases from 0.066 min^{-1} to 0.086 min^{-1} . These values are of the same order of magnitude than those obtained from mono-component solutions (Table 1).

In the case of POH-A₁PEI, a reciprocal trend is observed: the equilibrium is reached faster for La(III) (i.e., 15 min) than for Tb(III) (i.e., 25 min); this is also confirmed by a substantial difference in the apparent rate coefficients (0.26 min^{-1} for La(III) vs. 0.15 min^{-1} for Tb(III)). It is noteworthy that the apparent rate coefficient does not change for Tb(III) compared with mono-component solutions, while it increases by 55% for La(III). It is noteworthy that the cumulative sorption capacity for mono- and multi-component systems are comparable around 0.43 mmol g^{-1} , with a La/Tb repartition close to 60/40%: surprisingly, Tb(III) sorption capacity at equilibrium increased in bi-component solution compared with reference mono-component test, contrary to La(III) where a reciprocal trend is observed. In bi-component solutions, apparently the uptake kinetics is enhanced for La(III), while the sorption capacity is decreased in the presence of Tb(III).

A complementary study was focused on the sorption of La(III) and Tb(III) sorption in multi-component equimolar solutions at different pH_0 values (in the range 1–5), containing Si(IV), Ca(II) and Mg(II). Fig. 4

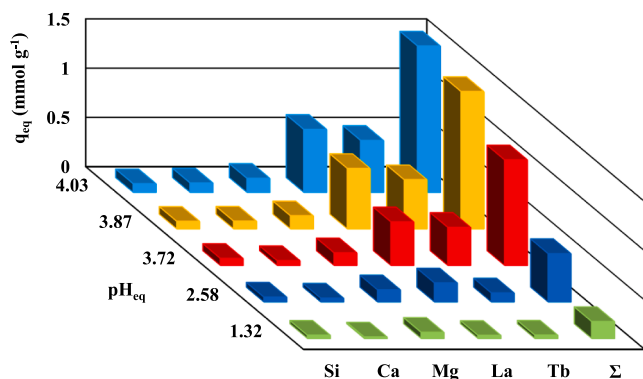


Fig. 4. Effect of equilibrium pH on the sorption of target metal ions from multi-component equimolar solutions using POH-A₁PEI sorbent (pH_0 : 1, 2, 3, 4 and 5; C_0 : 1 mmol metal L^{-1} ; SD: 0.75 g L^{-1} ; time: 10 h; T: $21 \pm 1 \text{ }^\circ\text{C}$).

confirms the strong preference of POH-A₁PEI for REEs over alkali-earth elements and Si(IV), regardless of the pH. As expected, the recovery of La(III) and Tb(III) (and other metal ions) increases with the pH. Consistently with previous results, POH-A₁PEI is more favorable for the sorption of La(III) (q_{eq} : 0.64 mmol La g^{-1}) than Tb(III) (q_{eq} : 0.53 mmol Tb g^{-1}) at pH_0 5 (pH_{eq} : 4.03). Figure S13 plots the \log_{10} of distribution ratios for selected metals vs. the pH: the slope of the correlation lines ranges between 0.64 and 0.73 for REEs; much higher than for other metals (less sensitive to pH and with much lower affinity). Figure S14 compares the selectivity coefficients ($\text{SC}_{\text{Me1/Me2}} = \text{D}_{\text{Me1}}/\text{D}_{\text{Me2}}$) for La(III) and Tb(III) over other metals. Increasing the pH improves both the sorption of REEs (Table S9 – semi-quantitative EDX analysis of sorbent surface) and the selectivity of the sorbent for REEs over alkali-earth metal ions and silica. The pH does not change the order of preference of the sorbent for selected metals. At pH_{eq} 4.03, POH-A₁PEI selectively recovers metal ions according the sequence: La(III) $>$ Tb(III) ($\text{SC}_{\text{La/Tb}}$: ~ 2.0) \gg Mg(II) (SC : ~ 21.5) \gg Ca(II) (SC : ~ 31.4) \gg Si(IV) (SC : ~ 37.2). Ca(II) and Mg(II) are also part of the hard acid class; the selectivity order was tentatively correlated with several ionic parameters (summarized in Table S4). Unfortunately, it was not possible to connect these trends with the physicochemical properties and apparently, the most important criterion for this selectivity scale is associated with the +2 charge of Ca(II) and Mg(II) vs. the trivalent charge of REEs (but not consistent with the high selectivity against silica).

3.2.6. Metal desorption – Kinetics and sorbent recycling

The desorption of loaded La(III) and Tb(III) was studied using a mixture of 0.2 M HCl and 0.5 M CaCl₂ solutions: the acid solution displaces the sorption equilibrium by metal release with the contribution of CaCl₂ (promoting ion-exchange). In addition, Ca(II) contributes to the stabilization of carboxylic acid groups (guluronic and mannuronic acids from algal and alginate compounds). The desorption is faster than for sorption: a contact time of 20 min is sufficient for achieving the complete elution of the metals both on A₁PEI and POH-A₁PEI (Figure S15) for sorbents loaded in mono-component solutions (25 min in the case of bi-component solutions, Figure S16), compared with 30–40 min for reaching the equilibrium in the case of uptake kinetics. The PFORE fits a little better kinetic profiles than the PSORE (Tables S10 and S11), consistently with the trends observed for uptake kinetics. The apparent rate coefficient for desorption ranges between 0.097 min^{-1} and 0.087 min^{-1} for A₁PEI, consistent with POH-A₁PEI/La(III) (i.e., 0.091–0.084 min^{-1}), and a little higher than for POH-A₁PEI/Tb(III) (i.e., 0.068–0.065 min^{-1}).

The high efficiency of the desorption step allows recovering the metal ions for further valorization, Table 4 reports the sorption and desorption performances for POH-A₁PEI sorbent recycling (five successive runs). After five runs, the sorption efficiency decreases by 8.7% for La(III) and 8.1% for Tb(III). The sorption is remarkably stable; this is consistent with the stability of the FTIR spectra (see Section 3.3.1.) that confirm that the successive sorption/desorption hardly change the typical bands of the sorbent. It is noteworthy that the complete elution of REEs is maintained over the five cycles: this highly efficient desorption

Table 4

Recycling of POH-A₁PEI – Cycles of sorption and desorption (SE: sorption efficiency, %; DE, desorption efficiency, %; StD: standard deviation, %).

Cycle #	Lanthanum				Terbium			
	SE	StD	DE	StD	SE	StD	DE	StD
1	82.5	1.3	100.0	0.1	76.4	1.1	100.3	0.3
2	81.7	1.5	100.2	0.4	75.0	1.0	100.2	0.7
3	79.5	0.1	99.8	0.2	73.3	2.2	100.6	0.4
4	77.3	0.3	100.2	0.2	72.3	2.2	100.1	0.0
5	75.3	0.1	99.3	0.4	70.2	1.0	99.9	0.0

Experimental conditions – Sorption: C_0 : 50 mg L^{-1} ; pH_0 : 5; SD: 0.666 g L^{-1} ; Time: 24 h; T: $20 \pm 1 \text{ }^\circ\text{C}$ / Desorption: 0.2 M HCl/0.5 M CaCl₂ eluent; SD: 2 g L^{-1} ; Time: 2 h; T: $20 \pm 1 \text{ }^\circ\text{C}$.

also contributes to the stability in sorption performance.

3.3. Ore treatment

3.3.1. Characterization of the ore

Table S2 reports the main constituents of the ore. It is noteworthy that the Egyptian ore collected in a sedimentary basin was characterized by a typical radiological anomaly. The chemical U content (analyzed by digestion and spectrophotometric measurement) was U_c : 411.7 mg U kg⁻¹ (average value collected from a broad study of geological samples, ranging between 390.9 and 570.7 mg U kg⁻¹). On the other side, the eU content (analyzed by field radiometry, using a Rs-230 BGO Super-Spec, Radiation Detection Systems AB, Backehagen, Sweden) showed a higher content, around 510 mg U kg⁻¹ (in the range 370–609 mg U kg⁻¹). The ratio U_c/eU was defined by Haskin et al., [65] for qualifying the “stability” (equilibrium state) of the geological formation (claystone). Here, the D-factor of Haskin is close to 0.81; this means that uranium is relatively stable in the mineral formation (limited migration). The eTh values varied between 15 and 57 ppm; the average value was around 34 ppm. The average value eU/eTh (Clark coefficient, [66]) is close to 15, much higher than the expected value for stabilized sedimentary deposit (i.e., 1). This means that the transfer of uranium leached from surrounding mineral formations enriches the deposit.

3.3.2. Heap leaching

The ore was processed using heap leaching (~0.5 M sulfuric acid solution): major elements are Al(III) (i.e., ~791 mg L⁻¹), Fe(III) (i.e., ~472 mg L⁻¹), Ca(II) (i.e., ~189 mg L⁻¹), Si(IV) (i.e., ~50 mg L⁻¹) (Table S12). In addition, the leachate contains high concentration of U(VI) (i.e., ~217 mg L⁻¹) and traces of REEs such as La(III) (i.e., ~13.7 mg L⁻¹) or Tb(III) (i.e., ~8.4 mg L⁻¹); the global REE index (measured by the spectrophotometric method) is close to 98 mg REE L⁻¹.

3.3.3. Pre-treatment by sorption on quaternary ammonium resin

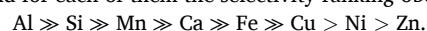
The leachates were pretreated by sorption on quaternary ammonium resin (QA resin). Table S12 shows the comparison of inlet and outlet concentrations for selected metal ions, and the extraction efficiency (%). The quaternary ammonium resin is highly efficient for uranium recovery (sorption efficiency ~ 94%); sulfuric acid leaching produces anionic species such as $[(UO_2)(SO_4)_3]^{4-}$, which are readily bound onto quaternary ammonium salt reactive groups at pH around 1.8. The residual concentration is close to 12.9 mg U L⁻¹. The other metal ions present in the solution are also partially bound (in the range 9.4–37.1%); the loss of

REEs does not exceed 20% (based on global REE index).

3.3.4. Metal sorption on POH-A₁PEI

The residual solution was then treated by sorption on POH-A₁PEI at different pH values (in the range pH₀: 1–5). Fig. 5 shows the sorption efficiency for selected metal ions: (a) the sorption efficiency drastically increases with the pH, (b) for strategic metals (i.e., U, La and Tb) the removal ranges between 86% and 92%, (c) for minor base metals (Zn, Cu, Ni) the recovery reaches 51–60%, and (d) the removal efficiency does not exceed 34% for other (major) elements. The sorbent maintains a good affinity for REEs, despite the presence of huge concentrations of Ca(II) (i.e., 153 mg Ca L⁻¹), Fe(III) (i.e., 299 mg Fe L⁻¹) or Al(III) (i.e., 618 mg Al L⁻¹). This is a confirmation of the strong affinity of POH-A₁PEI for REEs(III) and U(VI), despite the presence of large excess of base and alkali-earth metals. Obviously, the sorption capacities are influenced by the levels of concentrations of the metals in the leachates (Figure S17). As expected, the sorption capacities increase with pH and the higher sorption levels are roughly correlated with the concentrations levels of the metals (for the major elements) in the pre-treated leachate: Al>>Fe>>Ca>>Si > Ni > Mn > Zn≈Cu > La > U > Tb.

Figure S18 shows the selectivity coefficients of POH-A₁PEI for U(VI), La(III) and Tb(III) vs. competitor metals. The comparison of these selectivity coefficients shows that the sorbent has a preference for U(VI) > La(III) > Tb(III) against base and alkali-earth metals (and Si(IV)). The selectivity for each of these three strategic metals increases with the pH and for each of them the selectivity ranking obeys the series:



Although the main binding groups may be classified as hard bases and U(VI), La(III) and Tb(III) as hard acids, the sorbent shows a greater selectivity against hard acids (such as Al(III), Si(IV), Mn(II), Ca(II) and Fe(III)) than against borderline metal ions (such as Cu(II), Ni(II) and Zn(II)). Figure S19 and Table S13 show the semi-quantitative EDX analysis of the POH-A₁PEI surface after sorption of the pre-treated leachate at pH₀ 5; which shows that the sorbent has a remarkable concentrating effect (initial concentration in the solution and uptake on the sorbent). Despite the low concentrations of REEs in the solution, the atomic concentrations (%) are remarkably high. The levels are consistent with the capacities reported above. Most of the elements of the REE family are identified on the sorbent; it is noteworthy that the highest contributions come from heavy REEs (HREEs).

3.3.5. Metal desorption from metal-loaded sorbent

The elution of metal-loaded POH-A₁PEI with a 0.3 M HCl solution

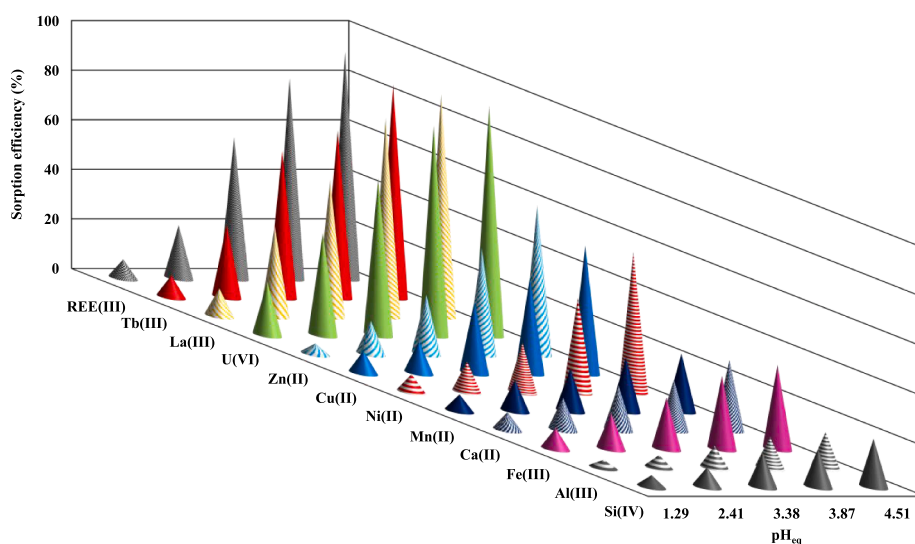


Fig. 5. Effect of pH on the sorption efficiency for target metals using POH-A₁PEI (after pre-treatment with QA-Resin) (SD: 2 g L⁻¹; agitation time: 5 h; T: 21 ± 2 °C, v: 165 ± 5 rpm.).

allows recovering >99% of all the metals bound on the sorbent. The procedure is not selective. Figure S20 shows the concentrations of selected elements in the eluate (for sorbents loaded at different pH values). The concentration levels in the eluate are consistent with their initial abundance in the leachates: major compounds in the eluates are Al(III), Fe(III), Ca(II) (concentrations ranging between 26 and 86 mmol L⁻¹), while the concentrations of minor elements range between 1 and 5 mmol L⁻¹, at pH₀ 5 (i.e., pH_{eq} 4.51).

3.3.6. Selective recovery of REEs from eluate by oxalic acid precipitation

The eluates were treated with oxalic acid solutions at pH 1.2 for selective precipitation of REEs [67–70]. Table S14 reports the residual concentrations of the metals after the precipitation step (for POH-A₁PEI sorbents loaded at pH₀ 4 and 5, at lower pH values, the amounts of REEs sorbed and then eluted are too low to make the precipitation efficient [71]).

The results confirm the high efficiency of the procedure for collecting REEs: 95–99% of REEs are recovered by oxalic acid precipitation (for sample processing at pH₀ 5 – pH_{eq} 4.51). On the other side, the loss of other metals remains negligible, in the range 10–17% (of the residual amounts in the eluate) except for Zn(II) (i.e., ~19%). Figure S21 confirms the “purity” of the REEs-oxalate precipitate (~71.7%, weight fraction): the semi-quantitative EDX analysis reports the presence of traces of N and Ca elements (<2.5%, in weight), in addition to C and O elements (from oxalate, ~25.9%). Figure S22 shows that the combination of elution and oxalate precipitation steps allows enriching substantially the proportion of specific REEs (i.e., Sm ≫ Nd ≫ Gd): for these REEs, the enrichment factor (i.e., EF) ranges between 7 and 15.5 times (close to 2 for Eu(III) and below 1.55 for the other elements of the REE series).

3.3.7. Treatment of residue (after REE oxalate precipitation) – Separation of Al/Fe and U(VI)

The residue of oxalic acid precipitation step contains substantial amounts of U(VI), Ca(II), Fe(III), Al(III) and Si(IV) (see Figure S23). The residual solution after oxalic acid precipitation contains uranium that can be recovered by precipitation. However, the effluent contains high concentrations of Al and Fe that could contaminate the yellow cake produced by U(VI) precipitation. A first step of precipitation (at pH 5) can be used for recovering these two major elements (i.e., Fe(III) and Al(III)). Table S15 confirms the high efficiency of aluminum and iron precipitation (higher than 91%), while the loss of other metals does not exceed 26% (around 11% for uranium; residual U(VI) concentration ~158 mg U L⁻¹). A final precipitation was processed at pH 9 for recovering uranium. Table S16 confirms that uranium can be removed almost quantitatively (i.e., around 97%) by pH control; the loss of other metals ranges between 11% and 32%. The semi-quantitative analysis of the yellow cake confirms the production of sodium uranate (Figure S24) associated with impurities, mainly constituted of organic residues (C: 11.4%, weight fraction, w.f.; 7.4% atomic fraction, at.f.) but also N (i.e., 10.5%, w.f. or 25.1% at.f.), and traces of iron, sodium, calcium, chlorine, and silicon (total: 18.5% w.f.; or 11.6% at.f.).

3.3.8. Flowsheet for the treatment of ore sample

Figure S25 summarizes the different steps of the processing of ore leachate. Fig. 6 shows the distribution of U, La, and Tb in the different compartments of the general processing of leachates (for sorbents applied at pH₀ 5, pH_{eq} 4.51). Uranyl is mainly recovered on the QA resin (94%), with a non-negligible fraction (i.e., close to 5%) passing through the oxalic acid precipitation step and collected into the precipitate at pH 9 (i.e., 4.3%). On the other side, REEs are mainly collected in the oxalic acid precipitate (71% for La(III) and 76% for Tb(III)), while the other significant fraction is immobilized on the QA resin (i.e., 17.9% for La(III) and 9.4% for Tb(III)).

The distributions of other metal ions (and Si) are reported in Figure S26. Most of these elements (i.e., 42–67%) are found in the outlet

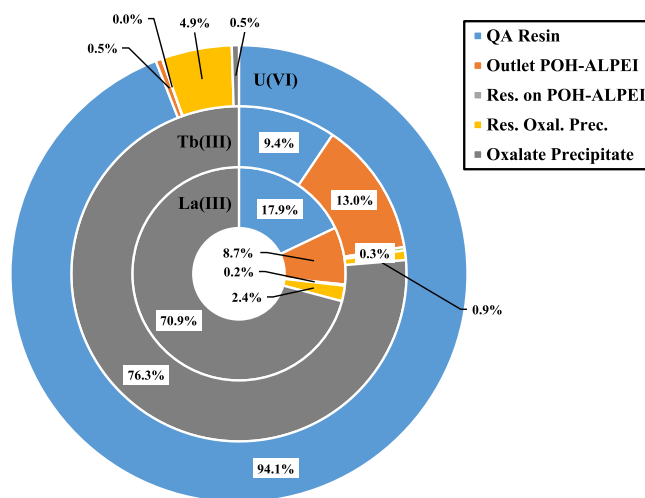


Fig. 6. Distribution of selected elements (U, La, and Tb) in the different compartments of the leachate processing (metal loading on the sorbent at pH_{eq}: 4.51).

of the sorption step on POH-A₁PEI, on the QA Resin (i.e., 19–37%), and in the residue of REE-oxalate precipitate (i.e., 10–19%). It is noteworthy that the fraction of these contaminants does not exceed 4% in the oxalate precipitates.

4. Conclusion

In this study, the new process of phosphorylation of algal/PEI beads (including the de-esterification step) produces a very efficient sorbent for the recovery of light and heavy rare earth elements from mild acid solutions. Sorption performance is significantly improved compared with raw support. Deprotonation of functional groups (i.e., phosphonate, amine and carboxylate groups) improves sorption of REEs. The sorption and desorption processes are fast: 20–30 min are enough for reaching equilibrium and complete elution of the two metals, respectively. The kinetic profiles are fitted by the pseudo-first order rate equation (higher correlation). The calculated values of the effective diffusivity are close to the self-diffusivity of the metal ions in water: the resistance to intraparticle diffusion does not play a significant role in the control of mass transfer and sorption kinetics. The Langmuir equation allows simulating sorption isotherms with high affinity and maximum sorption capacities close to 1.43 mmol La g⁻¹ and 1.02 mmol Tb g⁻¹ compared with the values reported for raw support; experimental maximum sorption capacities are lower than calculated capacities at saturation of the monolayer. The sorption performance (both apparent rate coefficient, sorption capacities and affinity coefficients) are increased by temperature: the sorption of REEs on POH-A₁PEI is endothermic and spontaneous.

Tested in equimolar multi-component solutions, the sorbent shows a preference for light REE against heavy REE, and even more against Mg(II) > Ca(II) ≈ Si(IV). Efficient metal desorption (using 0.2 M HCl/0.5 M CaCl₂) allows recycling the sorbent for a minimum of five cycles: the desorption efficiency remains higher than 99% while the sorption capacity decreases by <9% at the fifth cycle.

The high efficiency of the sorbent and its preferential affinity for REEs is finally demonstrated for the treatment of acidic leachates produced from the treatment of a sedimentary uranium-bearing ore. The acid leachates are pre-treated by sorption on a commercial quaternary ammonium resin (retaining 94% of U and 9–18% of REEs). Applied to this pre-treated leachates, the sorption on POH-A₁PEI is highly efficient for REEs; under selected experimental conditions and at pH₀: 5 (pH_{eq}: ~4.5), sorption efficiency ranges between 85 and 89% for Tb(III) and La(III), respectively. The desorption of loaded sorbents is totally achieved

(>99%, for U, REEs and other elements bound on the sorbent) using 0.3 M HCl solution. REEs can be recovered as oxalate precipitates at pH 1.5: 71% of La(III) and 76% of Tb(III) initially present in the leachate are recovered in the precipitate. The residual solution after oxalic acid precipitation step is pre-treated at pH 5 for precipitation of major metal ions (i.e., Al(III) and Fe(III)). A complementary fraction of U(VI) (i.e., 4.3% of initial amount of uranium) is recovered after a final precipitation step at pH 9. Semi-quantitative EDX analyses confirm the relative purity of the different precipitates, as a justification of the global separative treatment.

These results confirm the high efficiency of the sorbent for the recovery of REEs (with a preference for light REEs) even in the presence of large excess of other metal ions. The high stability of the sorption performances is another marker of the interest of this new material for the valorization of strategic metals, including uranyl recovery (as an additional target).

Declaration of Competing Interest

The authors declare that they have no known competing financial interests or personal relationships that could have appeared to influence the work reported in this paper.

Acknowledgements

E.G., and M.F.H., acknowledge Institut Français d'Égypte and Egyptian Academy of Science and Technology, Egypt for supporting the collaboration between IMT-Mines Ales and Nuclear Materials Authority, through IMHOTEP project "MetalValor" (ref. 39529QA). E.R.C. thanks the project RTI2018-099668-BC22 of Ministerio de Ciencia, Innovación y Universidades, the project UMA18-FEDERJA-126 of Junta de Andalucía, and FEDER funds.

Appendix A. Supplementary data

Supplementary data to this article can be found online at <https://doi.org/10.1016/j.cej.2021.130500>.

References

- [1] L. Omodara, S. Pitkäaho, E.-M. Turpeinen, P. Saavalainen, K. Oravisjärvi, R. L. Keiski, Recycling and substitution of light rare earth elements, cerium, lanthanum, neodymium, and praseodymium from end-of-life applications - a review, *J. Cleaner Prod.* 236 (2019) 117573, <https://doi.org/10.1016/j.jclepro.2019.07.048>.
- [2] S. Sinha, P. Abhilash, B.D. Meshram, Pandey, Metallurgical processes for the recovery and recycling of lanthanum from various resources-a review, *Hydrometallurgy* 160 (2016) 47–59.
- [3] N.-K. Ahn, H.-W. Shim, D.-W. Kim, B. Swain, Valorization of waste NiMH battery through recovery of critical rare earth metal: a simple recycling process for the circular economy, *Waste Manage. (Oxford)* 104 (2020) 254–261.
- [4] T. Kegl, A. Kosak, A. Lobnik, Z. Novak, A.K. Kralj, I. Ban, Adsorption of rare earth metals from wastewater by nanomaterials: a review, *J. Hazard. Mater.*, 386 (2020) Art. N° 121632.
- [5] D.L. Ramasamy, V. Puhakka, E. Repo, S. Khan, M. Sillanpää, Coordination and silica surface chemistry of lanthanides (III), scandium (III) and yttrium (III) sorption on 1-(2-pyridylazo)-2-naphthol (PAN) and acetylacetone (acac) immobilized gels, *Chem. Eng. J.* 324 (2017) 104–112.
- [6] V. Balaram, Rare earth elements: a review of applications, occurrence, exploration, analysis, recycling, and environmental impact, *Geosci. Front.* 10 (2019) 1285–1303.
- [7] S. Rangabhashiyam, K. Vijayaraghavan, Biosorption of Tm(III) by free and polysulfone-immobilized *Turbinaria conoides* biomass, *J. Ind. Eng. Chem.* 80 (2019) 318–324.
- [8] T.B. da Costa, M.G. Carlos da Silva, M.G. Adeodato Vieira, Recovery of rare-earth metals from aqueous solutions by bio/adsorption using non-conventional materials: a review with recent studies and promising approaches in column applications, *J. Rare Earths* 38 (2020) 339–355.
- [9] Z. Guo, Q. Li, Z. Li, C. Liu, X. Liu, Y. Liu, G. Dong, T. Lan, Y. Wei, Fabrication of efficient alginate composite beads embedded with N-doped carbon dots and their application for enhanced rare earth elements adsorption from aqueous solutions, *J. Colloid Interface Sci.* 562 (2020) 224–234.

- [10] D. Kolodynska, D. Fila, Z. Hubicki, Static and dynamic studies of lanthanum(III) ion adsorption/desorption from acidic solutions using chelating ion exchangers with different functionalities, *Environ. Res.*, 191 (2020) 110171–110171.
- [11] H. Javadian, M. Ruiz, T.A. Saleh, A.M. Sastre, Ca-alginate/carboxymethyl chitosan/Ni_{0.2}Zn_{0.2}Fe_{2.6}O₄ magnetic bionanocomposite: synthesis, characterization and application for single adsorption of Nd³⁺, Tb³⁺, and Dy³⁺ rare earth elements from aqueous media, *J. Mol. Liq.*, 306 (2020) Art. N° 112760.
- [12] H. Javadian, M. Ruiz, A.M. Sastre, Response surface methodology based on central composite design for simultaneous adsorption of rare earth elements using nanoporous calcium alginate/carboxymethyl chitosan microbionanocomposite powder containing Ni_{0.2}Zn_{0.2}Fe_{2.6}O₄ magnetic nanoparticles: batch and column studies, *Int. J. Biol. Macromol.* 154 (2020) 937–953.
- [13] N.K. Gupta, A. Gupta, P. Ramteke, H. Sahoo, A. Sengupta, Biosorption-a green method for the preconcentration of rare earth elements (REEs) from waste solutions: a review, *J. Mol. Liq.* 274 (2019) 148–164.
- [14] K. Vijayaraghavan, S. Rangabhashiyam, T. Ashokkumar, J. Arockiaraj, Assessment of samarium biosorption from aqueous solution by brown macroalga *Turbinaria conoides*, *J. Taiwan Inst. Chem. Eng.* 74 (2017) 113–120.
- [15] J. Jacinto, B. Henriques, A.C. Duarte, C. Vale, E. Pereira, Removal and recovery of critical rare elements from contaminated waters by living *Gracilaria gracilis*, *J. Hazard. Mater.* 344 (2018) 531–538.
- [16] N. Ferreira, A. Ferreira, T. Viana, C.B. Lopes, M. Costa, J. Pinto, J. Soares, J. Pinheiro-Torres, B. Henriques, E. Pereira, Assessment of marine macroalgae potential for gadolinium removal from contaminated aquatic systems, *Sci. Total Environ.* 749 (2020) 141488, <https://doi.org/10.1016/j.scitotenv.2020.141488>.
- [17] N.K. Gupta, B.C. Choudhary, A. Gupta, S.N. Achary, A. Sengupta, Graphene-based adsorbents for the separation of f-metals from waste solutions: a review, *J. Mol. Liq.*, 289 (2019) Art. N° 111121.
- [18] J. Roosen, J. Spooren, K. Binnemans, Adsorption performance of functionalized chitosan-silica hybrid materials toward rare earths, *J. Mater. Chem. A* 2 (45) (2014) 19415–19426.
- [19] S. Ravi, S. Zhang, Y.-R. Lee, K.-K. Kang, J.-M. Kim, J.-W. Ahn, W.-S. Ahn, EDTA-functionalized KCC-1 and KIT-6 mesoporous silicas for Nd³⁺ ion recovery from aqueous solutions, *J. Ind. Eng. Chem.* 67 (2018) 210–218.
- [20] R. Ahmad, Z. Ali, A.A. Khan, N.U. Rehman, Terbium extraction by functionalized surface: experimental and DFT approach, *Adsorption (J. Int. Ads. Soc.)* 26 (1) (2020) 117–125.
- [21] M.L. Rahman, M.S. Sarjadi, S.E. Arshad, M.M. Yusoff, S.M. Sarkar, B. Musta, Kenaf cellulose-based poly(amidoxime) ligand for adsorption of rare earth ions, *Rare Met.* 38 (3) (2019) 259–269.
- [22] H.M.H. Gad, M.M. Hamed, H.M.M. Abo Eldahab, M.E. Moustafa, S.A. El-Reefy, Radiation-induced grafting copolymerization of resin onto the surface of silica extracted from rice husk ash for adsorption of gadolinium, *J. Mol. Liq.* 231 (2017) 45–55.
- [23] J. Roosen, K. Binnemans, Adsorption and chromatographic separation of rare earths with EDTA- and DTPA-functionalized chitosan biopolymers, *J. Mater. Chem. A* 2 (5) (2014) 1530–1540.
- [24] F. Wang, J. Zhao, X. Wei, F. Huo, W. Li, Q. Hu, H. Liu, Adsorption of rare earths(III) by calcium alginate-poly glutamic acid hybrid gels, *J. Chem. Technol. Biotechnol.* 89 (7) (2014) 969–977.
- [25] K.A.M. Salih, M.F. Hamza, H. Mira, Y. Wei, F. Gao, A.M. Atta, T. Fujita, E. Guibal, Nd(III) and Gd(III) sorption on mesoporous amine-functionalized polymer/SiO₂ composite, *Molecules*, 26 (2021) Art. N° 26041049.
- [26] A.F. Abdel-Magied, H.N. Abdelhamid, R.M. Ashour, X. Zou, K. Forsberg, Hierarchical porous zeolitic imidazolate frameworks nanoparticles for efficient adsorption of rare-earth elements, *Microporous Mesoporous Mater.* 278 (2019) 175–184.
- [27] S. Ravi, Y.-R. Lee, K. Yu, J.-W. Ahn, W.-S. Ahn, Benzene triamido-tetraphosphonic acid immobilized on mesoporous silica for adsorption of Nd³⁺ ions in aqueous solution, *Microporous Mesoporous Mater.* 258 (2018) 62–71.
- [28] B. Maranescu, L. Lupa, A. Visa, Synthesis, characterization and rare earth elements adsorption properties of phosphonate metal organic frameworks, *Appl. Surf. Sci.* 481 (2019) 83–91.
- [29] Y. Wei, K.A.M. Salih, S. Lu, M.F. Hamza, T. Fujita, T. Vincent, E. Guibal, Amidoxime functionalization of algal/polyethyleneimine beads for the sorption of Sr(II) from aqueous solutions, *Molecules*, 24 (2019) Art. N° 3893.
- [30] M.F. Hamza, K.A.M. Salih, A.A.H. Abdel-Rahman, Y.E. Zayed, Y. Wei, J. Liang, E. Guibal, Sulfonic-functionalized algal/PEI beads for scandium, cerium and holmium sorption from aqueous solutions (synthetic and industrial samples), *Chem. Eng. J.*, 403 (2021) Art. N° 126399.
- [31] M.F. Hamza, S.M. Lu, K.A.M. Salih, H. Mira, A.S. Dhmees, T. Fujita, Y.Z. Wei, T. Vincent, E. Guibal, As(V) sorption from aqueous solutions using quaternized algal/polyethyleneimine composite beads, *Sci. Total Environ.*, 719 (2020) Art. N° 137396.
- [32] M.F. Hamza, A.E. Mubark, Y. Wei, T. Vincent, E. Guibal, Quaternization of composite algal/PEI beads for enhanced uranium sorption-application to ore acidic leachate, *Gels*, 6 (2020) Art. N° 6020012.
- [33] M.F. Hamza, Y. Wei, E. Guibal, Quaternization of algal/PEI beads (a new sorbent): characterization and application to scandium recovery from aqueous solutions, *Chem. Eng. J.*, 383 (2020) Art. N° 123210.
- [34] Y. Wei, K.A.M. Salih, M.F. Hamza, T. Fujita, E. Rodríguez-Castellón, E. Guibal, Synthesis of a new phosphonate-based sorbent and characterization of its interactions with lanthanum (III) and terbium (III), *Polymers*, 13 (2021) Art. N° 1513.

- [35] E.O. Opare, E. Struhs, A. Mirkouei, A comparative state-of-technology review and future directions for rare earth element separation, *Renewable & Sustainable Energy Reviews*, 143 (2021) Art. N° 110917.
- [36] RSC, Periodic Table, <https://www.rsc.org/periodic-table/>, Accessed: 5/10/2021.
- [37] S. Costis, K.K. Mueller, L. Coudert, C.M. Neculita, N. Reynier, J.F. Blais, Recovery potential of rare earth elements from mining and industrial residues: a review and cases studies, *J. Geochem. Explor.*, 221 (2021) Art. N° 106699.
- [38] F. Cucchiella, I. D'Adamo, S.C. Lenny Koh, P. Rosa, Recycling of WEEE: an economic assessment of present and future e-waste streams, *Renewable Sustainable Energy Rev.* 51 (2015) 263–272.
- [39] S. Costis, K.K. Mueller, J.-F. Blais, A. Royer-Lavallée, L. Coudert, C.M. Neculita, Review of recent work on the recovery of rare earth elements from secondary sources, in, *Natural Resources Canada, INRS, Centre - Eau Terre Environnement, Ottawa, ON, Canada*, 2019, pp. 63.
- [40] P. Josso, S. Roberts, D.A.H. Teagle, O. Pourret, R. Herrington, C. Ponce de Leon Albarran, Extraction and separation of rare earth elements from hydrothermal metalliferous sediments, *Miner. Eng.*, 118 (2018) 106–121.
- [41] M.F. Hamza, J.-C. Roux, E. Guibal, Uranium and europium sorption on amidoxime-functionalized magnetic chitosan micro-particles, *Chem. Eng. J.* 344 (2018) 124–137.
- [42] A.K. Nayak, A. Pal, Development and validation of an adsorption kinetic model at solid-liquid interface using normalized Gudermannian function, *J. Mol. Liq.* 276 (2019) 67–77.
- [43] E.C. Lima, A. Hosseini-Bandegharai, J.C. Moreno-Piraján, I. Anastopoulos, A critical review of the estimation of the thermodynamic parameters on adsorption equilibria. Wrong use of equilibrium constant in the Van't Hoff equation for calculation of thermodynamic parameters of adsorption, *J. Mol. Liq.* 273 (2019) 425–434.
- [44] T. Kegl, I. Ban, A. Lobnik, A. Košak, Synthesis and characterization of novel $\gamma\text{-Fe}_2\text{O}_3\text{-NH}_4\text{OH}@\text{SiO}_2(\text{APTMS})$ nanoparticles for dysprosium adsorption, *J. Hazard. Mater.*, 378 (2019) Art. N° 120764.
- [45] Z.R. Lopicic, M.D. Stojanovic, T.S.K. Radoicic, J.V. Milojkovic, M.S. Petrovic, M. L. Mihajlovic, M.L.J. Kijevcanin, Optimization of the process of Cu(II) sorption by mechanically treated *Prunus persica* L. - contribution to sustainability in food processing industry, *J. Cleaner Prod.* 156 (2017) 95–105.
- [46] Y. Cantu, A. Remes, A. Reyna, D. Martinez, J. Villarreal, H. Ramos, S. Trevino, C. Tamez, A. Martinez, T. Eubanks, et al., Thermodynamics, kinetics, and activation energy studies of the sorption of chromium(III) and chromium(VI) to a Mn_3O_4 nanomaterial, *Chem. Eng. J.* 254 (2014) 374–383.
- [47] W. Davies, W. Gray, A rapid and specific titrimetric method for the precise determination of uranium using iron(II) sulphate as reductant, *Talanta* 11 (1964) 1203–1211.
- [48] Z. Marczenko, Separation and spectrophotometric determination of elements, 2nd ed., Ellis Horwood, Chichester, UK, 1986, 678 pp.
- [49] R.C. Merritt, The extractive metallurgy of uranium, Colorado School of Mines Research Institute, Golden, CO, USA, 1971pp.
- [50] K. Li, M. Li, D. Xue, Solution-phase electronegativity scale: Insight into the chemical behaviors of metal ions in solution, *J. Phys. Chem. A* 116 (2012) 4192–4198.
- [51] M. Hubbe, S. Azizian, S. Douven, Implications of apparent pseudo-second-order adsorption kinetics onto cellulosic materials: a review, *BioResources* 14 (3) (2019) 7582–7626.
- [52] Y. Marcus, Ion properties, Marcel Dekker Inc, New York, NY, 1997, p. 259.
- [53] R.G. Pearson, Acids and bases 151 (1966) 172–177.
- [54] B. Rafik, O. Noureddine, A. Abderabbou, L. Habib, Self-diffusion coefficients of the trivalent f-element ion series in dilute and moderately dilute aqueous solutions: A comparative study between europium, gadolinium, terbium and berkelium, in: L. Rao, J.G. Tobin, D.K. Shuh (Eds.), *Actinides 2009*, IOP Publishing Ltd, Bristol (UK), 2010.
- [55] Y.J. Yang, S.D. Alexandratos, Affinity of polymer-supported reagents for lanthanides as a function of donor atom polarizability, *Ind. Eng. Chem. Res.* 48 (2009) 6173–6187.
- [56] S.D. Alexandratos, X. Zhu, The effect of hydrogen bonding in enhancing the ionic affinities of immobilized monoprotic phosphate ligands, *Materials*, 10 (2017) Art. N° 10080968.
- [57] M.E. Mahmoud, A.K. Mohamed, M.F. Amira, S.M. Seleim, Water-stable metal-organic framework/amine-modified silica/poly (piperazine-cresol) hybrids for efficient uptake of La(III) ions, *Mater. Chem. Phys.*, 251 (2020) Art. N° 123107.
- [58] K.Z. Elwakeel, A.M. Daher, A.I.L. Abd El-Fatah, H. Abd El Monem, M.M.H. Khalil, Biosorption of lanthanum from aqueous solutions using magnetic alginate beads, *J. Dispersion Sci. Technol.* 38 (2017) 145–151.
- [59] M.M.H. Khalil, M.S. Atrees, A.L.L. Abd El Fatah, H. Salem, R. Roshdi, Synthesis and application studies of chitosan acryloylthiourea derivative for the separation of rare earth elements, *J. Dispersion Sci. Technol.* 39 (2018) 605–613.
- [60] W. Hua, T. Zhang, M. Wang, Y. Zhu, X. Wang, Hierarchically structural PAN/UiO-66-(COOH)(2) nanofibrous membranes for effective recovery of Terbium(III) and Europium(III) ions and their photoluminescence performances, *Chem. Eng. J.* 370 (2019) 729–741.
- [61] M. Ceglowski, G. Schroeder, Preparation of porous resin with Schiff base chelating groups for removal of heavy metal ions from aqueous solutions, *Chem. Eng. J.* 263 (2015) 402–411.
- [62] A.B. Botelho Junior, E.F. Pinheiro, D.C.R. Espinosa, J.A.S. Tenorio, M.d.P.G. Baltazar, Adsorption of lanthanum and cerium on chelating ion exchange resins: kinetic and thermodynamic studies, *Sep. Sci. Technol.*, (2021) doi: 10.1080/01496395.01492021.01884720.
- [63] X. Chen, L. He, B. Liu, Y. Tang, The development of a material for uranium sorption in NH_3/N environments, *J. Radioanal. Nucl. Chem.* 307 (2016) 211–215.
- [64] V.J. Inglezakis, A.A. Zorpas, Heat of adsorption, adsorption energy and activation energy in adsorption and ion exchange systems, *Desalin. Water Treat.* 39 (2012) 149–157.
- [65] L.A. Haskin, M.A. Haskin, F.A. Frey, T.R. Wildeman, Relative and absolute terrestrial abundances of the rare earths, in: L.H. Ahrens (Ed.) *Origin and Distribution of the Elements*, Pergamon, 1968, pp. 889–912.
- [66] J.S.P. Clark, Z.E. Peterman, K.S. Heier, Section 24: abundances of uranium, thorium and potassium, in: J.S.P. Clark (Ed.) *Handbook of Physical Constants*, Geological Society of America, 1966.
- [67] R.G. Silva, C.A. Morais, L.V. Teixeira, É.D. Oliveira, Selective precipitation of high-quality rare earth oxalates or carbonates from a purified sulfuric liquor containing soluble impurities, *Min. Metall. Explor.* 36 (2019) 967–977.
- [68] F. Sadri, F. Rashchi, A. Amini, Hydrometallurgical digestion and leaching of Iranian monazite concentrate containing rare earth elements Th, Ce, La and Nd, *Int. J. Miner. Process.* 159 (2017) 7–15.
- [69] C. Tunsu, J.B. Lapp, C. Ekberg, T. Retegan, Selective separation of yttrium and europium using Cyanex 572 for applications in fluorescent lamp waste processing, *Hydrometallurgy* 166 (2016) 98–106.
- [70] E. Jorjani, M. Shahbazi, The production of rare earth elements group via tributyl phosphate extraction and precipitation stripping using oxalic acid, *Arabian J. Chem.* 9 (2016) S1532–S1539.
- [71] B. Hu, M. He, B. Chen, Z. Jiang, Separation/preconcentration techniques for rare earth elements analysis, *Physical Sciences Reviews*, 1 (2016) Art. N° 2016-0056.
- [72] A.C. Texier, Y. André, P. Le Cloirec, Selective biosorption of lanthanide (La, Eu) ions by *Mycobacterium smegmatis*, *Environ. Technol.* 18 (1997) 835–841.
- [73] L. Philip, L. Iyengar, C. Venkobachar, Biosorption of U, La, Pr, Nd, Eu and Dy by *Pseudomonas aeruginosa*, *J. Ind. Microbiol. Biotechnol.* 25 (2000) 1–7.
- [74] V. Diniz, B. Volesky, Effect of counterions on lanthanum adsorption by *Sargassum polycystum*, *Water Res.* 39 (2005) 2229–2236.
- [75] Ş. Sert, C. Kütahyalı, S. Inan, Z. Talip, B. Çetinkaya, M. Eral, Biosorption of lanthanum and cerium from aqueous solutions by *Platanus orientalis* leaf powder, *Hydrometallurgy* 90 (2008) 13–18.
- [76] R.C. Oliveira, O. Garcia, Jr., Study of biosorption of rare earth metals (La, Nd, Eu, Gd) by *Sargassum* sp biomass in batch systems: physicochemical evaluation of kinetics and adsorption models, in: E.R. Donati, M.R. Viera, E.L. Tavani, M.A. Giaveno, T.L. Lavallo, P.A. Chiacchiarini (Eds.) *Biohydrometallurgy: A Meeting Point between Microbial Ecology, Metal Recovery Processes and Environmental Remediation*, Trans Tech Publications, Switzerland, 2009, pp. 605–608.
- [77] Q. Chen, Study on the adsorption of lanthanum(III) from aqueous solution by bamboo charcoal, *J. Rare Earths* 28 (2010) 125–131.
- [78] D. Wu, J. Zhao, L. Zhang, Q. Wu, Y. Yang, Lanthanum adsorption using iron oxide loaded calcium alginate beads, *Hydrometallurgy* 101 (2010) 76–83.
- [79] K. Vijayaraghavan, M. Sathishkumar, B. Balasubramanian, Biosorption of lanthanum, cerium, europium, and ytterbium by a brown marine alga, *Turbinaria conoides*, *Ind. Eng. Chem. Res.* 49 (2010) 4405–4411.
- [80] M. Torab-Mostaedi, Biosorption of lanthanum and cerium from aqueous solutions using tangerine (*Citrus reticulata*) peel: equilibrium, kinetic and thermodynamic studies, *Chem. Ind. Chem. Eng. Q.* 19 (2013) 79–88.
- [81] M. Torab-Mostaedi, M. Asadollahzadeh, A. Hemmati, A. Khosravi, Biosorption of lanthanum and cerium from aqueous solutions by grapefruit peel: equilibrium, kinetic and thermodynamic studies, *Res. Chem. Intermed.* 41 (2) (2015) 559–573.
- [82] B. Esma, A. Omar, D.M. Amine, Comparative study on lanthanum(III) sorption onto Lewatit TP 207 and Lewatit TP 260, *J. Radioanal. Nucl. Chem.* 299 (1) (2014) 439–446.
- [83] M.M. Rahman, S.B. Khan, H.M. Marwani, A.M. Asiri, $\text{SnO}_2\text{-TiO}_2$ nanocomposites as new adsorbent for efficient removal of La(III) ions from aqueous solutions, *J. Taiwan Inst. Chem. Eng.* 45 (4) (2014) 1964–1974.
- [84] G. Hong, M. Wang, X. Li, L. Shen, X. Wang, M. Zhu, B.S. Hsiao, Micro-nano structure nanofibrous p-sulfonatocalix 8 arene complex membranes for highly efficient and selective adsorption of lanthanum(III) ions in aqueous solution, *RSC Adv.* 5 (2015) 21178–21188.
- [85] O.A. Oyewo, M.S. Onyango, C. Walkersdorfer, Lanthanides removal from mine water using banana peels nanosorbent, *Int. J. Environ. Sci. Technol.* 15 (6) (2018) 1265–1274.
- [86] E.M. Abu Elgoud, Z.H. Ismail, M.I. Ahmad, Y.A. El-Nadi, S.M. Abdelwahab, H. F. Aly, Sorption of lanthanum(III) and neodymium(III) from concentrated phosphoric acid by strongly acidic cation exchange resin (SQS-6), *Russ. J. Appl. Chem.* 92 (2019) 1581–1592.
- [87] A.E. Oral, S. Aytas, S. Yusan, S. Sert, C. Gök, O. Elmastas Gultekin, Preparation and characterization of a graphene-based magnetic nanocomposite for the adsorption of lanthanum ions from aqueous solution, *Anal. Lett.*, 53 (2020) 1812–1833.
- [88] N.S.G. Reddy, K.M. Rao, K.S.V.K. Rao, C.-S. Ha, Synthesis of 1-acryloyl-3-phenylthiourea based pH sensitive hydrogels for removal of samarium and terbium, *Macromol. Res.* 24 (2016) 494–501.